




## Article

# Mechanochemical Synthesis of Nanocrystalline Olivine-Type $\text{Mg}_2\text{SiO}_4$ and $\text{MgCoSiO}_4$

Phuong Q. H. Nguyen <sup>1</sup>, Warren McKenzie <sup>1</sup>, Dongzhou Zhang <sup>1,2</sup>, Jingui Xu <sup>1,2</sup>, Robert Rapp <sup>1</sup>, John P. Bradley <sup>1</sup> and Przemyslaw Dera <sup>1,\*</sup>

<sup>1</sup> Hawaii Institute of Geophysics and Planetology, University of Hawaii at Manoa, 1680 East-West Road, Honolulu, HI 96822, USA; nguyenph@hawaii.edu (P.Q.H.N.); warrenmc@hawaii.edu (W.M.); dzhang@hawaii.edu (D.Z.); xujingui@hawaii.edu (J.X.); rrappp@hawaii.edu (R.R.); johnbrad@hawaii.edu (J.P.B.)

<sup>2</sup> GeoSoilEnviroCARS, Argonne National Laboratory, University of Chicago, Argonne, IL 60439, USA

\* Correspondence: pdera@hawaii.edu; Tel.: +1-808-956-6347; Fax: +1-808-956-3188

**Abstract:** Nanocrystalline olivine-structured  $\text{Mg}_2\text{SiO}_4$  and  $\text{MgCoSiO}_4$ , with an average particle size of 27 nm and 31 nm, respectively, were successfully synthesized from oxide precursors via mechanochemical methods. The two nanocrystalline products were obtained after milling for 360 min and displayed high concentrations of  $\text{Mg}_2\text{SiO}_4$  (>94%) and  $\text{MgCoSiO}_4$  (>95%), together with minor amounts of WC (~3%) contaminant originating as debris abraded off milling balls and chambers. The macroscopic temperature monitoring of the grinding jars during milling trials recorded a peak temperature of 75 °C. A combination of analytical techniques that included XRD, TEM, SAED, and EDS were employed for the characterization of the synthesized products.

**Keywords:** mechanochemistry; nanocrystalline; olivine; mechanochemical synthesis; X-ray powder diffraction; forsterite; milling; solid solution



**Citation:** Nguyen, P.Q.H.; McKenzie, W.; Zhang, D.; Xu, J.; Rapp, R.; Bradley, J.P.; Dera, P.

Mechanochemical Synthesis of Nanocrystalline Olivine-Type  $\text{Mg}_2\text{SiO}_4$  and  $\text{MgCoSiO}_4$ . *Crystals* **2022**, *12*, 369. <https://doi.org/10.3390/cryst12030369>

Academic Editor: Arcady Zhukov

Received: 11 February 2022

Accepted: 7 March 2022

Published: 10 March 2022

**Publisher's Note:** MDPI stays neutral with regard to jurisdictional claims in published maps and institutional affiliations.



**Copyright:** © 2022 by the authors. Licensee MDPI, Basel, Switzerland. This article is an open access article distributed under the terms and conditions of the Creative Commons Attribution (CC BY) license (<https://creativecommons.org/licenses/by/4.0/>).

## 1. Introduction

Olivine-type orthosilicates  $(M,N)_2\text{SiO}_4$ , where  $M$  and  $N$  are mainly Fe and Mg, with small amounts of Co, Mn, Ca, and Ni present, represent a fundamental class of minerals of mafic and ultramafic igneous rocks in the crust and upper mantle of the Earth [1–3]. While forsterite ( $\text{Mg}_2\text{SiO}_4$ ) and fayalite ( $\text{Fe}_2\text{SiO}_4$ ) are the predominant end members, other binary silicates—i.e., larnite ( $\text{Ca}_2\text{SiO}_4$ ); liebenbergite ( $\text{Ni}_2\text{SiO}_4$ ); tephroite ( $\text{Mn}_2\text{SiO}_4$ ); and Ca-containing ternary silicates, i.e., kirschsteinite ( $\text{CaFeSiO}_4$ ), monticellite ( $\text{CaMgSiO}_4$ ), and glaucochroite ( $\text{CaMnSiO}_4$ )—are also naturally occurring minerals. The olivine structure is among the most robust crystallographic arrangements and able to accommodate a variety of metal cations, together with different types of anionic groups, i.e., germanate  $\text{GeO}_4^{2-}$ ,  $\text{SiS}_4^{2-}$ , phosphate  $\text{PO}_4^{3-}$ , and  $\text{GeS}_4^{2-}$  [4–7].

The naturally occurring solid solution series of olivine  $(\text{Fe}_{1-x}\text{Mg}_x)_2\text{SiO}_4$  has been the subject of intensive research for refractories, battery materials, mineralogy, and carbon sequestration [8–12].  $\text{Mg}_2\text{SiO}_4$  exists in three well-established equilibrium polymorphs: orthorhombic Pnma forsterite  $\alpha$ - $\text{Mg}_2\text{SiO}_4$ , orthorhombic Imma wadsleyite spinelloid  $\beta$ - $\text{Mg}_2\text{SiO}_4$ , and cubic Fd-3m spinel ringwoodite  $\gamma$ - $\text{Mg}_2\text{SiO}_4$  [13]. The transformation of  $\alpha$ - $\text{Mg}_2\text{SiO}_4$  to  $\beta$ - $\text{Mg}_2\text{SiO}_4$  and  $\gamma$ - $\text{Mg}_2\text{SiO}_4$  occurs at elevated pressure and temperature, yet both stabilize at ambient conditions upon quenching.

Natural olivines incorporate small amounts of Co; the parameters controlling this process, e.g., diffusion rates, and the effects of Co incorporation on the physical properties of olivine have also been studied [14,15]. The end member of the  $(\text{Mg,Co})_2\text{SiO}_4$  solid solution,  $\text{Co}_2\text{SiO}_4$ , is not a recognized mineral, but can be produced synthetically. It also exists in three polymorphic forms, analogous to  $\text{Mg}_2\text{SiO}_4$  phases. Ringwood et al. found that the transformation of  $\text{Co}_2\text{SiO}_4$  from the olivine structure to the ringwoodite structure

took place at 7 GPa and 700 °C, and Morimoto et al. reported on the syntheses and crystal-chemical relationships of the three  $\text{Co}_2\text{SiO}_4$  polymorphs [16,17].

Recently, olivine solid solutions,  $\text{Mg}M'\text{SiO}_4$  (where  $M' = \text{Fe, Co, Mn}$ ), have received renewed interest as potential cathode materials for rechargeable magnesium batteries due to their high theoretical energy densities. The synthesis of these olivine solid solution series utilizes various conventional methods including a combination of modified sol-gel, molten salt, and water-based solution chemistry, all of which involve multi-step synthesis, while some required heating to above 450 °C [18–24]. For example, Li et al. prepared  $\text{MgFeSiO}_4$  through a flux method utilizing stoichiometric amounts of  $\text{MgO}$ ,  $\text{FeC}_2\text{O}_4 \cdot 2\text{H}_2\text{O}$ , and  $\text{SiO}_2$  and heat treatment at >800 °C in a controlled Ar atmosphere [19]. Qafoku et al. reported the synthesis of nanosized Fe(II)-rich olivine, fayalite,  $(\text{Mg}_{0.33}\text{Fe}_{0.66})_2\text{SiO}_4$ , and  $(\text{Mg}_{0.66}\text{Fe}_{0.33})_2\text{SiO}_4$ , using a metal ion-sucrose solution approach, with calcination at >850 °C under a flow of  $\text{CO}_2/\text{CO}/\text{Ar}$  balanced gas mixture and the removal of excess iron metal from isopropanol suspensions [23]. Feng et al. prepared  $\text{Mg}_{1.03}\text{Mn}_{0.97}\text{SiO}_4$  by milling a stoichiometric mixture of  $\text{MgO}$ ,  $\text{MnCO}_3$ , and  $\text{SiO}_2$ , followed by sintering at 900 °C for 24 h [18]. Mori et al. synthesized  $\text{MgMnSiO}_4$  using a flux method, starting from a 1:1:1 molar ratio mixture of  $\text{MgO}$ ,  $\text{MnCO}_3$ , and  $\text{SiO}_2$  ball-milled in ethanol at 300 RPM with subsequent calcination at >500 °C under a flux of 3%  $\text{H}_2/\text{Ar}$  balance [24]. Nuli et al. and Zheng et al. synthesized  $\text{MgCoSiO}_4$  utilizing water-based solution chemistry and a molten salt/mixed solvothermal approach in combination with heat treatment at 1000 °C and 1300 °C, respectively [20,21].

Mechanochemical synthesis by high-energy ball milling has become an important solid-state synthesis method for the production of nanomaterials, with advantages including large-scale capabilities (grams) and low reaction temperatures. The one-pot synthesis of olivine-type  $\text{Fe}_2\text{SiO}_4$  highlights the early work of Šepelák et al., starting from  $\text{Fe}_2\text{O}_3$ , Fe, and  $\text{SiO}_2$  and milled under Ar inert atmosphere [25]. Mechanochemically synthesized nanocrystalline  $\text{Co}_2\text{SiO}_4$  has also been reported recently by our lab using a 2:1 molar ratio mixture of  $\text{CoO}$  and  $\text{SiO}_2$  [26]. In an effort to standardize the Mg-Co silicate solution series preparation, we report here the results of our investigation into the mechanochemical synthesis of olivine-type  $\text{Mg}_2\text{SiO}_4$  and ternary olivine  $\text{MgCoSiO}_4$ , starting with stoichiometric amounts of  $\text{MgO}$ ,  $\text{SiO}_2$  and  $\text{CoO}$ ,  $\text{MgO}$ ,  $\text{SiO}_2$ , respectively.

## 2. Experimental Methods

**General Experimental Details.** All sample loading was conducted on a benchtop under ambient conditions. Powder XRD analysis of the substrates revealed that the  $\text{CoO}$  material contained 12.88 wt.% of spinel-structured mixed-valence cobalt oxide,  $\text{Co}_3\text{O}_4$  (known as mineral guite) (see Supplementary Materials Figure S1).  $\text{SiO}_2$  starting material was analyzed in the same manner as the cobalt oxide and was found to consist of pure phase  $\alpha$ -quartz with no measurable impurities (see Supplementary Materials Figure S2). Prior to the mechanochemical processing, the  $\text{MgO}$  starting material was heat-treated at 400 °C for 4 h to dehydrate any  $\text{Mg}(\text{OH})_2$  that was formed upon reacting with water in the ambient atmosphere. Powder XRD analysis of the sample after heat treatment indicated a high concentration of periclase  $\text{MgO}$  phase with trace amount of calcite  $\text{CaCO}_3$  (see Supplementary Materials Figure S3).

**Powder X-ray Diffraction (PXRD).** The sample was analyzed by high-resolution X-ray powder diffraction on a Bruker D8 Advance diffractometer with a 3 kW  $\text{CuK}\alpha$  source and a LynxEye XE detector in Bragg–Brentano parafocusing geometry, mounted on a 9-position automated sample changer using either standard puck-type mounts or zero-background Si-wafer mounts when only a small quantity of the processed sample was available. A 0.020 mm Ni filter was used to reduce  $\text{CuK}\beta$  radiation. Typical powder scans were conducted over a range of 5–85 degrees with a step size of 0.02 degrees and an exposure time of 1 s per step.

**Rietveld refinement analysis.** Rietveld analysis was conducted using Bruker TOPAS 5 [27]. Starting models of  $\text{MgCoSiO}_4$ ,  $\text{Mg}_2\text{SiO}_4$ ,  $\text{SiO}_2$ , WC,  $\text{CoWO}_4$ ,  $\text{Co}_3\text{O}_4$ ,  $\text{MgSiO}_3$ ,  $\text{MgO}$ , and  $\text{CaCO}_3$  structures were taken from PDF 04-017-1377, PDF 00-034-0189, PDF 00-046-1045, PDF 04-001-2755, PDF 00-015-0867, PDF 00-042-1467, COD 9007016, PDF 00-045-0946, and PDF 00-066-0867, respectively [28]. Refinement included the optimization of background, phase fractions, unit cell parameters, peak profiles (controlled by grain size and strain models), site occupancies for non-oxygen atoms, and atomic displacement parameters. Fractional atomic coordinates were kept fixed at literature values.

**Transmission Electron Microscopy (TEM).** In order to determine the elemental composition and to assess the chemical homogeneity of the final milled product, we used an 80–300 keV high-base Titan (FEI Thermo-Fisher) scanning transmission electron microscope equipped with a solid-state Si(Li) energy-dispersive X-ray detector (Genesis 4000, EDAX). Brightfield and darkfield images were acquired in scanning transmission (“STEM”) mode and the crystal structures of grains were assessed using selected area electron diffraction (SAED). Compositions were measured by energy-dispersive X-ray spectroscopy (“EDS”) and quantified using a Cliff–Lorimer thin-film approximation and correction factors (“K factors”) derived from thin-film standards. This procedure assumes that the specimen is sufficiently thin that any X-ray absorption by the specimen is minimal.

**Preparation of  $\text{Mg}_2\text{SiO}_4/\text{MgCoSiO}_4$ .** The synthetic procedure was based on the methodology developed previously by our group for the synthesis of the nanocrystalline  $\text{Co}_2\text{SiO}_4$  [26]. A mixture of a 2:1 molar ratio of magnesium oxide (0.62 g) and silicon oxide (0.47 g) and a second mixture of a 1:1:1 molar ratio of magnesium oxide (0.25 g), cobalt oxide (0.47 g), and silicon oxide (0.37 g) were loaded into 2 separate 25 mL tungsten carbide (WC) jars and mechanically milled under dry conditions with two 15 mm diameter WC balls (40:1 ball to powder ratio) oscillating at a frequency of 30 Hz for various durations of time, ranging from 0 to 360 min. Milling experiments performed in air or under a controlled atmosphere (Ar) produced no difference in the processing outcomes.

### 3. Results and Discussion

To set up a baseline methodological approach, forsterite  $\text{Mg}_2\text{SiO}_4$  was prepared by the high-energy milling of a 2:1 molar ratio mixture of  $\text{MgO}$  and  $\text{SiO}_2$  for 180 min. Our synthesis follows the general procedure of Nguyen et al. for the synthesis of olivine  $\text{Co}_2\text{SiO}_4$  [26]. Figure 1 illustrates the results of the Rietveld refinement of 180 min milled  $\text{Mg}_2\text{SiO}_4$ , which converge to a final figure of merit  $R_{\text{wp}} = 6.524$ . Small quantities of unreacted quartz  $\text{SiO}_2$  (3.03%) and qusongite WC (2.68%) that were shaved off the milling media were detected alongside the  $\text{Mg}_2\text{SiO}_4$  (94.29%). A good agreement between calculated and measured diffraction patterns was obtained based on the Rietveld refinements. The average crystallite size for the synthesized  $\text{Mg}_2\text{SiO}_4$  forsterite, based on the Rietveld refinement, was 26 nm.

Figure 2 shows a comparison between the powder XRD patterns of the product from the 1:1:1 molar ratio mixture of  $\text{MgO}$ ,  $\text{CoO}$ , and  $\text{SiO}_2$  milled for different lengths of time. Short milling times (up to 45 min) only produced changes in the average grain size of the sample and lattice strain, which are indicated by the increasing diffraction peak width, but no new peaks were observed. It was also observed that  $\text{MgO}$  turns amorphous after 15 min into milling. A weak pattern of orthorhombic olivine  $\text{MgCoSiO}_4$ , indicated by the characteristic peak at  $35.7^\circ$ , was observed after 90 min of milling time. The formation of  $\text{MgCoSiO}_4$  from this starting mixture was complete after 360 min of milling, as indicated by the complete disappearance of the strong  $\text{SiO}_2$  quartz diffraction peak at  $26.8^\circ$ . The diffraction peak width of the product phase is similar to that of the peaks of the precursors after 45 min of milling, indicating sub-micrometer grain sizes. WC debris, produced by the wear of the grinding elements, was also detected in the final product.

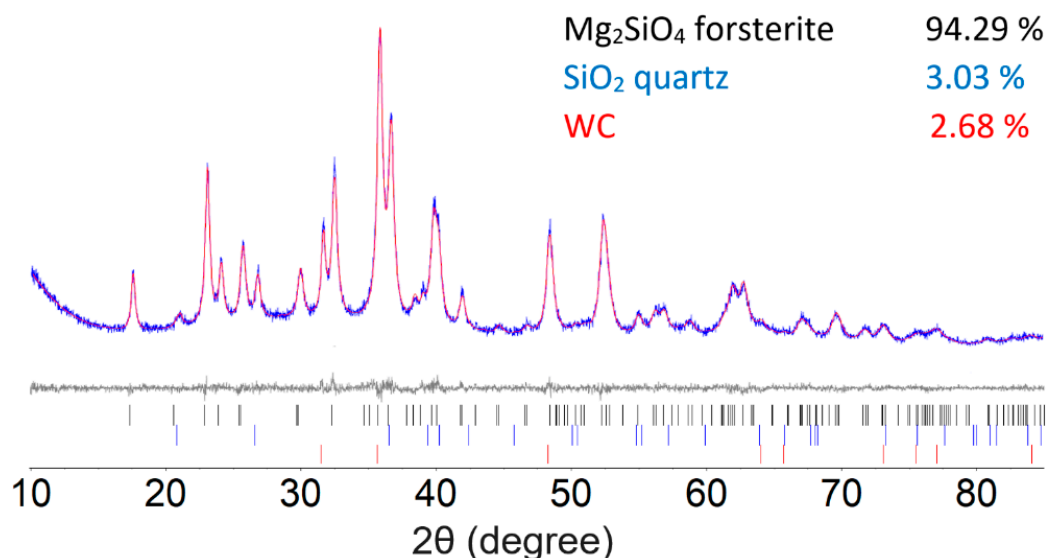


**Figure 1.** The Rietveld refinement of the 2:1 molar ratio of MgO and SiO<sub>2</sub> after 180 min of milling time. The bottom curve shows the difference between the observed and the calculated intensities. Tick marks below indicate the peak positions for Mg<sub>2</sub>SiO<sub>4</sub>, unreacted SiO<sub>2</sub>, and WC.

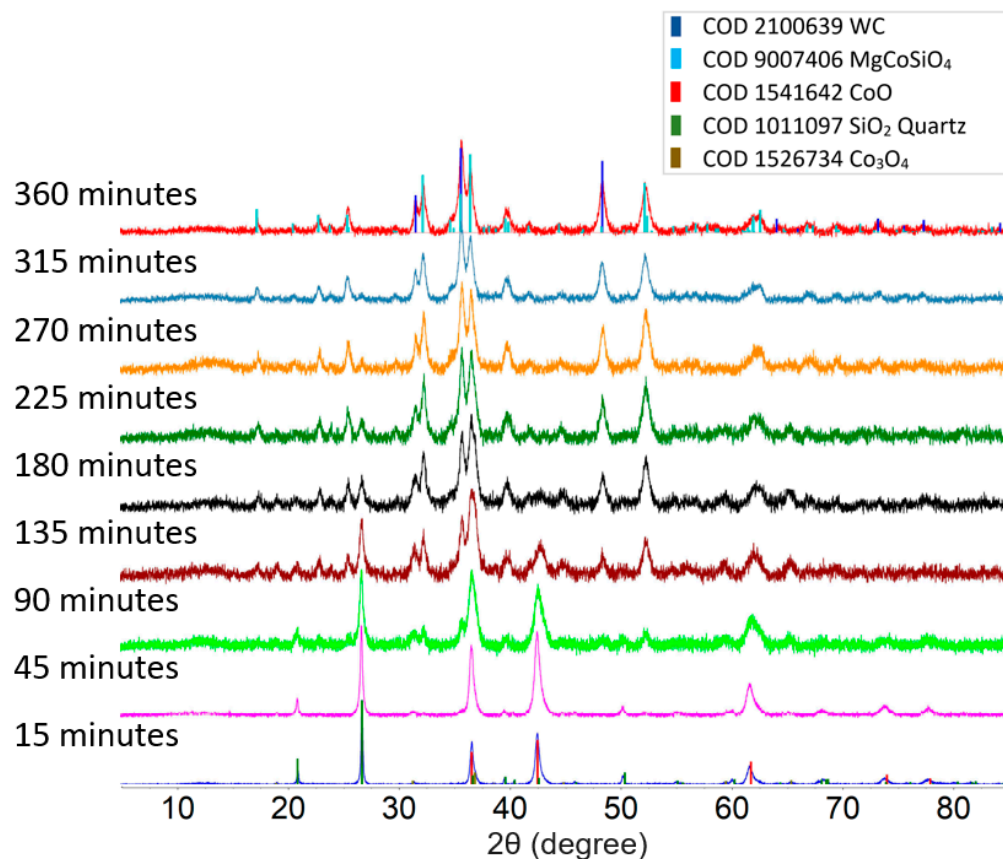


**Figure 2.** Powder XRD pattern of 1:1:1 molar ratio of MgO, CoO, and SiO<sub>2</sub> mixture after various milling times. MgO turns amorphous after milling for 15 min.

The milling process in an oscillating mill is believed to proceed at only slightly elevated average temperatures (<100 °C), although significant localized heating may occur from individual ball and sample impacts [29,30]. Attempts to monitor the temperature of the milling jar with an attached thermocouple registered that a maximum temperature of 75 °C

was reached during the milling trials. We further investigated the effect of temperature on the synthesized  $\text{MgCoSiO}_4$  olivine by annealing the milled powder at  $1000\text{ }^\circ\text{C}$  for 12 h.

Figure 3 illustrates the results of the Rietveld refinements on the 360 min milled samples with and without subsequent annealing, which converge to final figures of merit  $R_{\text{wp}} = 2.219$  and  $2.906$ , respectively. The Rietveld refinements of powder both before and after the annealing display marked changes in the peak width of the olivine phase, signifying grain growth. Annealing at  $1000\text{ }^\circ\text{C}$  further induced a side reaction of the WC debris with the olivine  $\text{MgCoSiO}_4$  sample, resulting in minor impurities of  $\text{CoWO}_4$  (1.07%) in the final product. Unreacted quite  $\text{Co}_3\text{O}_4$  (0.05%) and clinoenstatite  $\text{MgSiO}_3$  (3.60%) were also detected as minor phases. Unit cell parameters of olivine  $\text{Mg}_{2-x}\text{Co}_x\text{SiO}_4$  ( $x = 0, 0.5, 1$ ) show the expected linear trend of composition, confirming the successful diffusion of Mg and Co into the olivine lattice (Table 1). Further analysis of the occupancies on the M1 (edge-sharing tetragonally elongated octahedra) and M2 (corner-sharing trigonally elongated octahedra) metal sites suggests a strong preference for  $\text{Co}^{2+}$  over Mg on the M1 site in both annealed and unannealed samples. Annealing after milling further promoted the diffusion of  $\text{Mg}^{2+}$  into the M2 site, resulting in an increase in the Mg site occupancy factor from 0.591 to 0.675 on M2. Unit cell parameters of samples with and without annealing are comparable to literature values [17,31–35].

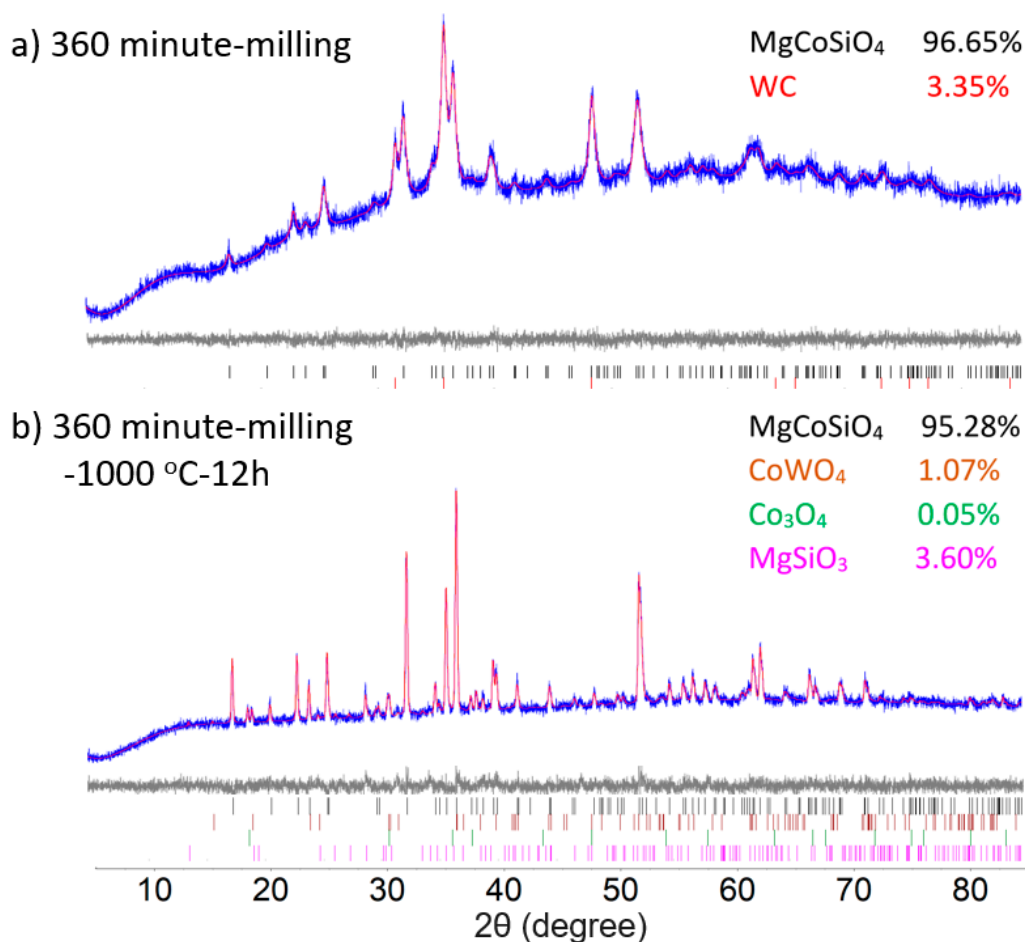


**Figure 3.** Rietveld refinement of the (a) 1:1:1 molar ratio of MgO, CoO and  $\text{SiO}_2$  after (a) 360 min milling time and (b) 360 min milled mixture followed by heating at  $1000\text{ }^\circ\text{C}$  for 12 h. The bottom curve shows the difference between the observed and the calculated intensities. Tick marks below indicate the peak positions for cobalt silicate and WC/ $\text{CoWO}_4$ .

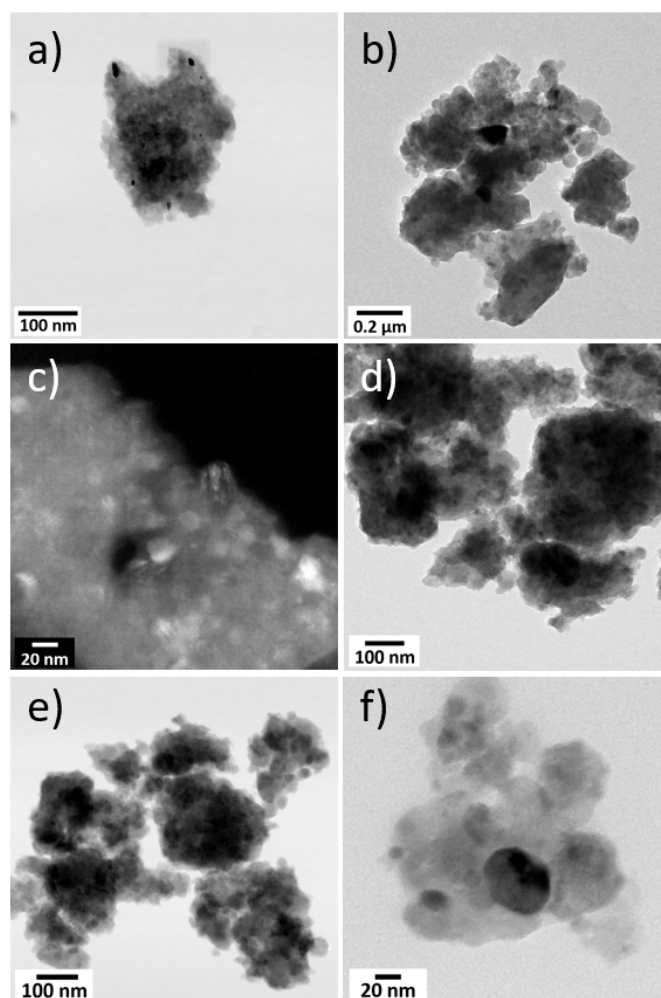


**Table 1.** Unit cell parameters obtained from the Rietveld refinement of the synthesized  $\text{MgCoSiO}_4$  before and after heating in comparison with literature values.

	This Study			Literature					
	$\text{Mg}_2\text{SiO}_4$	$\text{MgCoSiO}_4$		$\text{Mg}_2\text{SiO}_4$	$\text{Mg}_2\text{SiO}_4$	$\text{MgCoSiO}_4$	$\text{MgCoSiO}_4$	$\text{MgCoSiO}_4$	$\text{Co}_2\text{SiO}_4$
	360 min	360 min	Milled-1000 °C	Matsui et al. 1400 °C [31]	Akimoto et al. 1700 °C [32]	Rinaldi et al. 1200 °C [33]	Miyake et al. 1500 °C [34]	Sommer et al. 1200 °C [35]	Morimoto et al. 1500 °C [17]
a (Å)	4.756 (6)	4.77 (3)	4.775 (2)	4.7553 (6)	4.756 (1)	4.77572 (8)	4.771 (1)	4.7713 (1)	4.782 (4)
b (Å)	10.224 (12)	10.26 (7)	10.267 (5)	10.1977 (14)	10.197 (1)	10.27159 (17)	10.245 (1)	10.2533 (2)	10.302 (4)
c (Å)	5.993 (7)	5.99 (4)	5.999 (3)	5.9820 (7)	5.982 (1)	6.00235 (10)	5.988 (1)	5.9911 (2)	6.003 (4)
V (Å <sup>3</sup> )	291.4 (6)	294 (3)	294.1 (2)	290.09 (11)	290.1	294.441 (6)		293.09 (3)	
[Co_1]	0	0.606 (17)	0.637 (13)			0.698 (9)	0.675 (2)	0.666 (2)	
[Co_2]	0	0.409 (11)	0.325 (11)			0.302 (9)	0.278 (21)	0.334	
Si-O (Å)	1.639 (2)	1.642 (5)	1.6428 (1)				1.638		1.627
* M-O (Å)	2.115 (5)	2.122 (1)	2.1233 (1)				2.113		2.134
R <sub>wp</sub>	6.525	2.219	2.906				2.131		

Standard deviations in parentheses are in unit of the last digit \*; M = Mg/Co, [Co\_1] = Co atomic occupancy in M1 site.

TEM images of the synthesized  $\text{Mg}_2\text{SiO}_4$  product, obtained at different magnifications, are compared to synthetic  $\text{MgCoSiO}_4$  in Figure 4. The particle size for  $\text{MgCoSiO}_4$  ranged from 23 to 50 nm (average 27 nm), while a greater size variation between 8 to 67 nm (average 31 nm) was observed in  $\text{Mg}_2\text{SiO}_4$ . Many of the particles appeared to be present as clumps, signifying aggregation during milling. Attempts to break apart these clumps ultrasonically produced little change in the end product.

**Figure 4.** Brightfield and darkfield STEM images at different magnifications of the synthesized  $\text{Mg}_2\text{SiO}_4$  (a–c) and  $\text{MgCoSiO}_4$  (d–f).

The milled samples (Figure 5) showed high degrees of spottiness in the diffraction rings, consistent with the polycrystalline nature of the as-synthesized  $\text{Mg}_2\text{SiO}_4$  and  $\text{MgCoSiO}_4$ . The indexing of the SAED patterns revealed signature orthorhombic olivine crystal structures. The EDS analysis of selected particles of the 180 min milled  $\text{Mg}_2\text{SiO}_4$  indicated the presence of (as expected) Mg, Si, and O, as well as trace amounts of Ca (from  $\text{CaCO}_3$  in the MgO starting material), and Co as a carryover contaminant from previous milling trials (where a small amount of Co embedded itself in the WC grinding components) (Figure 6). Quantitative analysis of elemental mass percentages based on the EDS spectrum suggested an empirical formula of  $\text{Mg}_2\text{SiO}_4$ . EDS analysis of the  $\text{MgCoSiO}_4$  sample, although within the margin of error of the measurement, indicated some degree of variation in the Mg:Co:Si proportions. For example, the Mg:Si ratio of forsterite was 2.03:1; the Mg:Co:Si ratios of  $\text{MgCoSiO}_4$  covered the range of (0.61–0.93):(0.67–0.81):1. The amount of Si detected by XRD was significantly lower than that determined from the EDS analysis of the synthesized  $\text{MgCoSiO}_4$ . This could be due to selective (X-ray) absorption or to a residual amorphous Si-containing component that was not readily detected by XRD analysis [36].

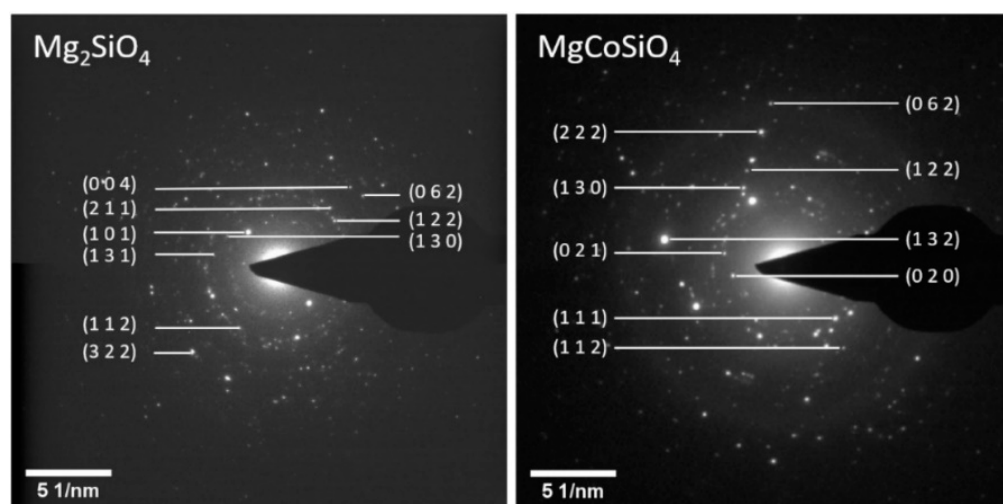


**Figure 5.** Selected area electron diffraction (SAED) images of synthesized  $\text{Mg}_2\text{SiO}_4$  (left) and  $\text{MgCoSiO}_4$  (right).

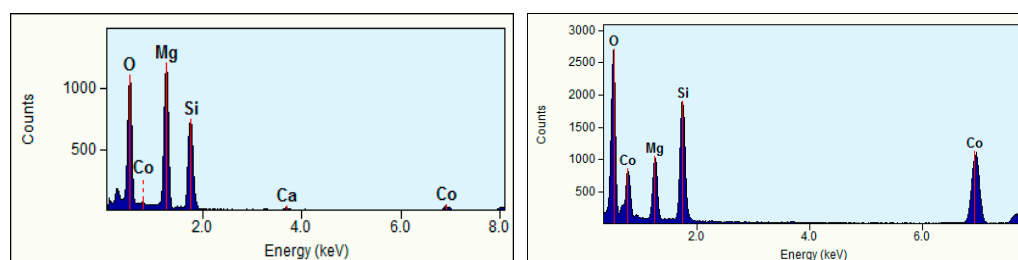


**Figure 6.** Representative STEM-EDS spectra of 360 min milled  $\text{Mg}_2\text{SiO}_4$  (left) and 360 min milled  $\text{MgCoSiO}_4$  (right).

#### 4. Conclusions

This report presents a straightforward method for synthesizing nanocrystalline  $\text{Mg}_2\text{SiO}_4$  and  $\text{MgCoSiO}_4$ . The ability to synthesize and finetune the chemical series of  $\text{Mg}^{2+}$  and  $\text{Co}^{2+}$  represents a unique contribution to olivine reactivity research. The synthesis technique was shown to be efficient at ambient temperatures, without contingent inert atmospheric control. Given the nanocrystalline nature of the products and the simple reaction activation by milling, research on a potential application, i.e., the battery performance testing of the mechanochemically synthesized  $\text{Mg}_2\text{SiO}_4$  and  $\text{MgCoSiO}_4$ , is currently underway. The

contamination of the synthesized olivine with WC, which in turn resulted in the undesirable formation of tungstate when annealing the milled product at an elevated temperature, remains an unresolved concern for further material development. Thus, a robust method for removing WC from mechanically synthesized olivine is necessary and will be addressed in a follow-up publication.

**Supplementary Materials:** The following supporting information can be downloaded at: <https://www.mdpi.com/article/10.3390/cryst12030369/s1>, Figure S1: Rietveld refinement of starting material CoO; Figure S2: Rietveld refinement of starting material SiO<sub>2</sub>; Figure S3: Rietveld refinement of starting material MgO.

**Author Contributions:** Conceptualization, P.Q.H.N. and P.D.; methodology, P.Q.H.N., P.D. and J.P.B.; data curation, P.Q.H.N., P.D. and J.P.B.; resources, P.D. and J.P.B.; writing—original draft preparation, P.Q.H.N. and P.D.; writing—review and editing, W.M., D.Z., J.X., R.R. and J.P.B. All authors have read and agreed to the published version of the manuscript.

**Funding:** Office of Naval Research, Department of Navy's Historically Black Colleges and Universities/Minority Institutions, the Materials for Thermal and Chemical Extreme program, grant number FOA N00014-19-S-F004 and NSF EAR grant 1829273.

**Institutional Review Board Statement:** Not applicable.

**Informed Consent Statement:** Not applicable.

**Data Availability Statement:** Not applicable.

**Acknowledgments:** We acknowledge the financial support of this work provided by the Office of Naval Research, Department of Navy's Historically Black Colleges and Universities/Minority Institutions, the Materials for Thermal and Chemical Extreme program, grant number FOA N00014-19-S-F004. R.R. has been supported by NSF EAR grant 1829273.

**Conflicts of Interest:** There are no conflict to declare.

## References

1. Anderson, D.L.; Bass, J.D. Mineralogy and composition of the upper mantle. *Geophys. Res. Lett.* **1984**, *11*, 637–640. [[CrossRef](#)]
2. McDonough, W.F.; Rudnick, R.L. Mineralogy and composition of the upper mantle. *Rev. Mineral.* **1998**, *37*, 139–164.
3. Rudnick, R.L.; Fountain, D.M. Nature and composition of the continental crust: A lower crustal perspective. *Rev. Geophys.* **1995**, *33*, 267–309. [[CrossRef](#)]
4. Volkov, N.V.; Mikhashenok, N.V.; Sablina, K.A.; Bayukov, O.A.; Gorev, M.V.; Balaev, A.D.; Pankrats, A.I.; Tugarinov, V.I.; Velikanov, D.A.; Molochev, M.S.; et al. Magnetic phase diagram of the olivine-type Mg<sub>2</sub>GeO<sub>4</sub> single crystal estimated from magnetic, resonance and thermodynamic properties. *J. Phys. Condens. Matter* **2013**, *25*, 136003. [[CrossRef](#)]
5. Masquelier, C.; Croguennec, L. Polyanionic (phosphates, silicates, sulfates) framework as electrode materials for rechargeable Li (or Na) batteries. *Chem. Rev.* **2013**, *113*, 6552–6591. [[CrossRef](#)]
6. Ericsson, T.; Amcoff, O.; Kalinowski, M. Cation preferences in thio-olivines (Fe<sub>1-x</sub>Mg<sub>x</sub>)<sub>2</sub>SiS<sub>4</sub>, x ≤ 0.30, studied by Mossbauer spectroscopy at room temperature. *Neues Jb. f. Mineral. Mh.* **1999**, *11*, 518–528.
7. Chung, J.-H.; Ohgushi, K.; Ueda, Y. Magnetic phase diagram of the multicritical olivine Mn<sub>2</sub>SiS<sub>4</sub> and Mn<sub>2</sub>GeS<sub>4</sub>. *J. Magn. Magn. Mater.* **2010**, *322*, 832–837. [[CrossRef](#)]
8. Goldschmidt, V. Olivine and forsterite refractories in Europe. *Ind. Eng. Chem.* **1938**, *30*, 32–34. [[CrossRef](#)]
9. Pack, A.; Hoernes, S.; Walther, T.; Bross, R. Behavior of basic refractories at high temperatures in steelmaking processes—thermodynamics and implications for the usability of olivine as refractory material. *Eur. J. Mineral.* **2003**, *15*, 193–205. [[CrossRef](#)]
10. Routschka, G. *Refractory Materials: Pocket Manual; Design, Properties, Testing*; Vulkan-Verlag GmbH: Essen, Germany, 2008.
11. Guo, H.; Ping, H.; Hu, J.; Song, X.; Zheng, J.; Pan, F. Controllable synthesis of LiFePO<sub>4</sub> in different polymorphs and study of the reaction mechanism. *J. Mater. Chem. A* **2017**, *5*, 14294–14300. [[CrossRef](#)]
12. Montserrat, F.; Renforth, P.; Hartmann, J.; Leermakers, M.; Knops, P.; Meysman, F.J. Olivine dissolution in seawater: Implications for CO<sub>2</sub> sequestration through enhanced weathering in coastal environments. *Environ. Sci. Technol.* **2017**, *51*, 3960–3972. [[CrossRef](#)]
13. Katsura, T.; Ito, E. The system Mg<sub>2</sub>SiO<sub>4</sub>-Fe<sub>2</sub>SiO<sub>4</sub> at high pressures and temperatures: Precise determination of stabilities of olivine, modified spinel, and spinel. *J. Geophys. Res. Solid Earth* **1989**, *94*, 15663–15670. [[CrossRef](#)]
14. Morioka, M. Cation diffusion in olivine—I. Cobalt and magnesium. *Geochim. Cosmochim. Acta* **1980**, *44*, 759–762. [[CrossRef](#)]
15. Chakraborty, S. Diffusion coefficients in olivine, wadsleyite and ringwoodite. *Rev. Mineral. Geochem.* **2010**, *72*, 603–639. [[CrossRef](#)]
16. Ringwood, A. Olivine-spinel transformation in cobalt orthosilicate. *Nature* **1963**, *198*, 79–80. [[CrossRef](#)]



17. Morimoto, N.; Tokonami, M.; Watanabe, M.; Koto, K. Crystal structures of three polymorphs of  $\text{Co}_2\text{SiO}_4$ . *Am. Mineral.* **1974**, *59*, 475–485.
18. Feng, Z.; Yang, J.; NuLi, Y.; Wang, J.; Wang, X.; Wang, Z. Preparation and electrochemical study of a new magnesium intercalation material  $\text{Mg}_{1.03}\text{Mn}_{0.97}\text{SiO}_4$ . *Electrochem. Commun.* **2008**, *10*, 1291–1294. [[CrossRef](#)]
19. Li, Y.; Nuli, Y.; Yang, J.; Yilinuer, T.; Wang, J.  $\text{MgFeSiO}_4$  prepared via a molten salt method as a new cathode material for rechargeable magnesium batteries. *Chin. Sci. Bull.* **2011**, *56*, 386–390. [[CrossRef](#)]
20. NuLi, Y.; Zheng, Y.; Wang, Y.; Yang, J.; Wang, J. Electrochemical intercalation of  $\text{Mg}^{2+}$  in 3D hierarchically porous magnesium cobalt silicate and its application as an advanced cathode material in rechargeable magnesium batteries. *J. Mater. Chem.* **2011**, *21*, 12437–12443. [[CrossRef](#)]
21. Zheng, Y.; NuLi, Y.; Chen, Q.; Wang, Y.; Yang, J.; Wang, J. Magnesium cobalt silicate materials for reversible magnesium ion storage. *Electrochim. Acta* **2012**, *66*, 75–81. [[CrossRef](#)]
22. Orikasa, Y.; Masese, T.; Koyama, Y.; Mori, T.; Hattori, M.; Yamamoto, K.; Okado, T.; Huang, Z.-D.; Minato, T.; Tassel, C. High energy density rechargeable magnesium battery using earth-abundant and non-toxic elements. *Sci. Rep.* **2014**, *4*, 5622. [[CrossRef](#)] [[PubMed](#)]
23. Qafoku, O.; Ilton, E.S.; Bowden, M.E.; Kovarik, L.; Zhang, X.; Kukkadapu, R.K.; Engelhard, M.H.; Thompson, C.J.; Schaefer, H.T.; McGrail, B.P.; et al. Synthesis of nanometer-sized fayalite and magnesium-iron(II) mixture olivines. *J. Colloid Interface Sci.* **2018**, *515*, 129–138. [[CrossRef](#)] [[PubMed](#)]
24. Mori, T.; Masese, T.; Orikasa, Y.; Huang, Z.-D.; Okado, T.; Kim, J.; Uchimoto, Y. Anti-site mixing governs the electrochemical performances of olivine-type  $\text{MgMgSiO}_4$  cathodes for rechargeable magnesium batteries. *Phys. Chem. Chem. Phys.* **2016**, *18*, 13524–13529. [[CrossRef](#)] [[PubMed](#)]
25. Šepelák, V.; Myndyk, M.; Fabián, M.; Da Silva, K.L.; Feldhoff, A.; Menzel, D.; Ghafari, M.; Hahn, H.; Heitjans, P.; Becker, K.D. Mechanochemical synthesis of nanocrystalline fayalite,  $\text{Fe}_2\text{SiO}_4$ . *Chem. Commun.* **2012**, *48*, 11121–11123. [[CrossRef](#)] [[PubMed](#)]
26. Nguyen, P.Q.H.; Zhang, D.; Rapp, R.; Bradley, J.P.; Dera, P. Room temperature facile synthesis of olivine- $\text{Co}_2\text{SiO}_4$  nanoparticles utilizing a mechanochemical method. *RSC Adv.* **2021**, *11*, 20687–20690. [[CrossRef](#)]
27. Coelho, A.A. TOPAS and TOPAS-Academic: An optimization program integrating computer algebra and crystallographic objects written in C++. *J. Appl. Crystallogr.* **2018**, *51*, 210–218. [[CrossRef](#)]
28. Gates-Rector, S.; Blanton, T. The powder diffraction file: A quality materials characterization database. *Powder Diffr.* **2019**, *34*, 352–360. [[CrossRef](#)]
29. Schmidt, R.; Scholze, H.M.; Stolle, A. Temperature progression in a mixer ball mill. *Int. J. Ind. Chem.* **2016**, *7*, 181–186. [[CrossRef](#)]
30. Takacs, L.; McHenry, J. Temperature of the milling balls in a shaker and planetary mills. *J. Mater. Sci.* **2006**, *41*, 5246–5249. [[CrossRef](#)]
31. Matsui, Y.; Syono, Y. Unit cell dimensions of some synthetic olivine group solid solutions. *Geochem. J.* **1968**, *2*, 51–59. [[CrossRef](#)]
32. Akimoto, S.I.; Fujisawa, H. Olivine-spinel solid solution equilibria in the system  $\text{Mg}_2\text{SiO}_4$ - $\text{Fe}_2\text{SiO}_4$ . *J. Geophys. Res.* **1968**, *73*, 1467–1479. [[CrossRef](#)]
33. Rinaldi, R.; Gatta, G.; Artioli, G.; Knight, K.; Geiger, C. Crystal chemistry, cation ordering and thermoelastic behaviour of  $\text{CoMgSiO}_4$  olivine at high temperature as studied by in situ neutron powder diffraction. *Phys. Chem. Miner.* **2005**, *32*, 655–664. [[CrossRef](#)]
34. Miyake, M.; Nakamura, H.; Kojima, H.; Marumo, F. Cation ordering in Co-Mg olivine solid-solution series. *Am. Mineral.* **1987**, *72*, 594–598.
35. Müller-Sommer, M.; Hock, R.; Kirfel, A. Rietveld refinement study of the cation distribution in (Co,Mg)-olivine solid solution. *Phys. Chem. Miner.* **1997**, *24*, 17–23. [[CrossRef](#)]
36. Sohor, M.A.H.M.; Mustapha, M.; Mamat, X. *The Effect of Milling Duration on Silicon Dioxide Characterization*; MATEC Web of Conferences; EDP Sciences: Les Ulis, France, 2017; p. 03007.